F-7

Micro-Structure of Hard Materials Deformed and Fractured under High Pressure

Shuichiro Takahashi, Naoto Asami,[1]
Yutaka Honda and Bumpei Ishii

Abstract

Microstructure study combined with X-ray analysis and measurement of micro-hardness was done for investigation of fracture phenomena and deformed structure under high pressure of the hard materials. The following results were obtained;

1. Even hard material became ductile under high environmental pressure.
2. The softening and re-precipitation of carbide were observed in the case of the hardened carbon steel which has near the maximum hardness of the material deformed under high pressure.
3. The hardness of the tungsten carbide and carbon steel which has lower value increased by deformation.

These results are discussed by the consideration of the diagram among environmental pressure, shear stress, true strain and temperature.

Introduction

Macroscopic study on fracture and ductility under high pressure had been conducted by many investigators.[1)2)3)] However, there are few studies on the micro-aspects of hard materials deformed and/or fractured under high pressure. For investigation of fracture phenomena and ductility at high stress, a microscopic study of fractured surfaces and deformed structures under the consideration of macro and micro stress systems is important, because local and/or massive structure changes or chemical diffusion at the stress concentrated domain can be expected.

Electron microscopic observation combined with optical microscopy, X-ray diffraction study, and the measurement of micro-hardness were done on the deformed and fractured hard materials, which had been loaded up to 20,000 ~ 300,000 bar at room temperature in Bridgman's, Drickamer's, tetrahedral and belt type high pressure equipments.

---

1. Mitsubishi Atomic Power Industries, Inc., Engineering and Research Laboratory, Ohmiya City, Saitama, Japan

As typical hard materials, three kinds of high carbon steel, {52100 and SUJ-2 (1% C, 1.45% Cr), SK-3 (1.05% C)} and three kinds of tungsten carbide-cobalt alloys (WC-3% Co, WC-3.5% Co, WC-6% Co) were selected. The chemical composition of the specimens are shown in Table 1.

Experiments and Results

High Carbon Steel

52100 steel and SUJ-2 steel bearing balls, on which top and bottom surfaces were flattened, were loaded in a form of Bridgman's anvil as shown Fig 1-(1); an SK-3 ring was compressed up to 20 kb in a piston cylinder system. The 52100 steel bearing balls, having Vickers hardness number (VH) of about 1,000 by quenching and heat treatment before the loading, failed at about 120 kb as one conical fragment having a glossy surface (Fig 1-(2)) and several fragments of brittle fractured mat surfaces. The top surface and the section crossing the central axis of the conical fragment were ground on a water cooled grinder and polished (Fig 1-(3)), and then chemically etched with 5% nital solution for 30 sec, or electrolytically etched in a bath of 10% chromate solution using 4 Volts D.C. for 2 min (Fig 1-(2)).

I) Aspect of materials in domain under nearly hydrostatic pressure.

In the domain (A) (Fig 1) where materials were pressed nearly hydrostatically and plastic deformation did not take place, the material showed the aspect of normal structure (Fig 2 domain A) predicted by simple thermodynamical consideration. A few exceptional structural changes occurred in grain boundaries, subgrain boundaries and precipitations, due to localized stress fields caused by nonuniformity such as crystal boundaries or precipitate. Furthermore, the hardness of the material in this domain (A) was not changed (Fig 3).

II) Aspect in the domain plastically deformed by high pressure gradient and under high hydrostatic pressure.

II-1) For specimens of nearly the maximum hardness of matrix (for example; 52100 - carbon steel having an original hardness about 1,000 VH), domain (B) (Fig 1) neighboring domain (A) had a large pressure gradient, and the material of this domain (B) is considered to undergo high pressure deformation. The hardness of domain (B) decreases with increasing pressure to a value of about 500 VH (Fig 3).

Resistivity against etchants (both Nital and chromate) was low compared to domains (A), (C) and (E). Microstructure of domain (B) showed that: (i) primary granular cementite precipitated at the grain boundary of Austenite became smaller than that of the original state, and was smaller than cementite located in domains (A), (C) and (E);

(ii) the small secondary granular cementites in Austenite grains in the original state were almost disappeared; (iii) a large amount of "fine needle cementite" was observed in the matrix (Fig 2 - domain B). These fine needle cementites had no relationship to granular cementites; (iv) a large amount of pores having different distribution in each domains(A), (B) and (C) were observed as showin in Fig 1 - (3).[2]

In Fig 3, the relationship between pore volume and distance from the top surface in the axial direction is compared with the relationship between hardness and distance. The relationship between pore distribution and hardness in the radial direction from the center to the outside at the top surface was very similar to this axial character. It must be noted that the pore distribution, hardness pattern and structure change are closely inter-related.

II-2) For materials, with original hardness below the maximum value of the matrix (for example, the SUJ-2 bearing steel with original hardness of 830 VH) the "softening process" mentioned above did not occur in the initial stage. Work hardening took place, and hardness reached 1,000 VH; abnormal changes of microstructure were not apparent. However, when pressurized further, the hardness of the material reached the maximum value of the matrix (due to the work hardening), followed by the softening process; the minimum hardness of the piece under the Bridgman anvil was 740 VH (Fig 5).

III) Aspect in the domain of low environmental pressure.

At the outside domain (E) (Fig 1) where the pressure was not high, the fractured surface showed brittle fracture clearly, and the structure was similar to the original one (Fig 4 - (1)).

IV) Fracture surface in the domain under high shear stress and high environmental pressure.

Fig 4-(2), (3), (4) show typical aspects of the fractured surface of the conical failed fragment of the 52100 bearing steel such as the domain D in Fig 1. This domain D was exposed to high shearing stress and hydrostatic pressure. Fig 4-(2) and (3) are electron micrographs of as-fractured surfaces in this domain. Fig 4-(4) is the same surface as in Fig 4-(1) and (3) after etching. The structure of those surfaces was clearly different from the normal brittle fractured surface as in Fig 4-(1), and large and small segregated carbides were observed in the flowed matrix.

Similar phenomena were observed in the material SK-3 tool steel, having an original hardness of about 900 VH. The hardness of this material decreased to 400 VH by deformation under compressive stress (Fig 6).

---

2. Arrow marked rectangular pores are indentor marks by micro-hardness test.

Fig 7-(3) shows the fractured surface structure of SK-3 steel, which was applied by shearing under compression 20 kb. Fig 7-(4) is an etched surface of the same specimen as in Fig 7-(3). Large and small precipitates were also observed in the extensively flowed matrix. The aspect of material sheared under high stress was clearly different from normal fractured surfaces as shown in Fig 7-(1) and (2) which show a surface as fractured and an etched surface of the same specimen.

Polished and etched surface near the fractured domain is shown in Fig 8-(1), (2), (3) and (4).

WC-Co Alloy

WC-3% Co alloy anvils were pressed up to 300 kb and were deformed in the form of Drickamer's type high pressure equipment shown in Fig 9-b, (D-type). The top of the anvil was deformed by pressure to a concave depth of 13μ. This highly deformed top domain looks like a "eye" on the fractured surface, and several isobaric lines were observed macroscopically. Micro-Vickers hardness (1,000 g load) was measured on the polished and lapped surface of a section crossing the center axis. The result is shown in Fig 10. The hardness was increased to 2800 VH near the top, decreased to the original hardness (2250 VH) at 4 mm in depth.

Fig 11-(1) is an electron-micrograph of the surface of WC-3% Co alloy anvil fractured at low hydrostatic pressure, Fig 11-(2) is a typical fractured surface of the domain deformed mainly by compression under the environmental pressure of 300 kb, and Fig 11-(3) a larger deformed portion.

The belt-type anvil (WC-3.5% Co alloy) was exposed to not only high hydrostatic pressure but also to high shear stress (Fig 9-a). Therefore, the distinct "high shear-stress fracture" took place, as shown in the bright fracture surface in Fig 9-a'. The electron micrograph (Fig 12-(2)) of this surface was smooth similar to that of carbon steel.

Fig 12-(3) and (4) are electron micrographs of WC-etched and Co-etched surfaces of the same specimen as in Fig 12-(2). In these pictures, the distinct precipitation of cobalt in small and large sizes was observed in the greatly flowed matrix.

These abnormal aspects became more demonstrative on the high shear-stress fractured surface of WC-6% Co alloy. Fig 13 shows typical pictures of the etched surface of a tetrahedral anvil fractured by shear force under 100 kb.

Fig 14 shows X-ray diffraction patterns of three fractured fragments. The line broadening was more remarkable for a glossy surface of the same specimen as in Fig 12, fractured by a high shear-

stress.

The sharpest line was from the as-received specimen, and the partially diffuse line was from the mat surface of fragments resulting from failure by low shear-high pressure.

Discussion

1) It is useful to consider first the linear relationship between true strain at fracture and hydrostatic pressure as shown in Fig 15 (upper) as originally determined by Bridgman by tension tests in the environment of high pressure liquid. Even brittle material becomes ductile above the transition pressure, the ductility increasing linearly with pressure. The diagram of the high pressure system used in one of the present experiments is illustrated with a general conceptual diagram in Fig 15 (lower).

In order to consider the problems of deformation and fracture of the actual stressed solid material, it is important to consider the stress system microscopically as well as macroscopically. If we take Bridgman's relationship into account, the stress set up in a small region of the solid material is to be divided into two main parts, namely, environmental hydrostatic pressure, Pe.h., and shear-stress, σ.

In Fig 15 (lower), the horizontal axis denotes environmental hydrostatic pressure, Pe.h., and the vertical axis shear-stress σ. The stresses of the representative regions (A), (B), (C) and (D) are shown on this Pe.h. — σ diagram. The horizontal solid line represents yield stress σ_Y, while the vertical broken line represents brittle to ductile transition pressure Pt. The degree of expected deformation is also shown on this diagram.

2) In the experimental result of 52100 carbon steel, it is estimated that the pressure gradient in the domain (B) is very large, being largest at the domain boundary of (B) and (A), and decreasing gradually toward domain (C).

So it can be expected that ductility of some pressurized region (such as domain (B)).of the mechanical system increases with the environmental hydrostatic pressure. Furthermore when "high pressure deformation" took place the large number of defects in thermal nonequilibrium were nucleated due to the large deformation. It is quite natural to expect these defects to contribute to the carbon diffusion from carbide (in this case cementite) to matrix, because the carbide is highly soluble in the iron base matrix under the conditions of high pressure with large pressure gradient and deformation. Large numbers of pores are clearly observed in domain (B), and the pore volume (or the number of pores) increases with increasing pressure gradiemt. It is also noted (Fig 3), that the hardness distribution curve is inversely proportional to pore volume distribution. The vacancies, which are generated during the "high pressure deformation",

will migrate and form pores. On the other hand, carbon atoms diffuse from the carbide into the matrix and reprecipitate as new small needles or dot carbides, as shown Fig 2-(2), domain (B).

For precipitate hardened material, for which hardness reached its maximum hardness, this linear relationship is modified as a result of modified structure due to chemical change described above. Precipitation hardened high carbon steel (such as 52100 steel) will increase its ductility initially along the P-e line of Pt-R-Q, but after stress exceeds the yield stress in the environment hydrostatic pressure, the ductility will increase abruptly due to the above mentioned structure change, and then increase along the P-e line of (Pt'-R'-Q'). So the actual deformation may take place along an P-e line of (Pt-R-R'-Q').

3) The microstructure of high carbon steel fractured at lower than the transition pressure Pt (transition of brittle to ductile) shows a typical "brittle" fracture, as in Fig 4-(1).

When the environment pressure is a little higher than the transition pressure Pt, the microstructure of fractured surface is very irregular as shown in Fig 7-(1), (2) and ductile domains are located at the stress concentrated portions, which are clearly indicated by the disappearance of carbide in pearlite structure on the etched surface Fig 7-(2). This local change at the stress concentrated portion is more clearly observed in Fig 8 which shows sections of same material of Fig 7.

4) When the environmental pressure is higher than Pt and the shear stress is greater than the yield stress, σ_Y, (domain D in the general conceptual diagram), the "abruptly deformation" mentioned above takes place and large number of minute incipient crack or void are considered to be generated nearly simultaneously. Large shearing stresses may concentrate near the end of initial crack voids. In this domain, very high stress is considered to develop locally, and highly ductile deformation and then fracture occur. Heat also generates in this band. This temperature rise may induce further deformation (Fig 16 P-T-e conceptual diagram). Thus, these deformation and heat generation induce the increased solubility of carbon in the iron matrix (in the case of carbon-iron alloys) and cobalt in the tungsten carbide matrix (in the case of tungsten carbide-cobalt alloys). This kind of fracture is seen in the conical fracture of 52100 steel (named domain D in Fig 4-(2), (3) and (4)), the surface of SK-3 fractured by high shear stress and pressure (Fig 7-(3) and (4)), the glossy fractured surfaces of WC-3.5% Co (B-type anvil, Fig 12-(2), (3) and (4)) and the glossy fractured surfaces of WC-6% Co (Fig 13).

Highly deformed structure of the matrix in this domain is also indicated by X-ray line broadening of WC-6% Co alloy, as in Fig 14. And the reason of the size and shape or pattern of reprecipitates are naturally considered as highly localization of the stress and disappearance of grain boundary on the fractured surface.

5) In the conical fragment, domains (A) and (C) are nearly hydrostatic regions. Therefore, deformation can scarcely be expected, with the exception of in the small stress concentrated regions such as near the grain boundaries; the extent of deformation is expected to depend on the pressure. In purely hydrostatic pressure, the diffusion decreases with pressure. Therefore, in these regions structural changes also are hardly to be expected.

Thus, the structure changes near the grain boundary in domain (A), and in a few parts of domain (C), are considered natural results of stress conditions (Fig 1-(3)). Furthermore, this local change near the grain boundary is one of the factors which promotes the abrupt deformation and fracture of the domain (D).

Conclusion

Brittle material under environmental hydrostatic high pressure becomes ductile. When shear stress is applied on the material in the environment, fracture occurs accompanied with plastic deformation, generation of non-equilibrium lattice defects, enhancement of atomic diffusion, and chemical change including dissolving and re-precipitation.

Further study is needed to extend these qualitative results to a quantitative basis, and to obtain a general solution for the problems of fracture and deformation of materials.

Acknowledgement

The authors are grateful to Mr. H. Uchikoshi for the X-ray measurement and to Mr. M. Yamada for the assistance of the high pressure experiments. The authors wish to thank Dr. A. Ookawa, Professor of Gakushuin University, and Dr. H. Doi, Central Research Laboratory of Mitsubishi Mining and Metallurgical Company, for their valuable discussions throughout the work.

Also, the authors acknowledge to Dr. M. Yokosuka, Director, and Mr. K. Sugimoto, Vice-director of our laboratory, for their support and permission to publish the work.

References

1) P.W. Bridgman,
"Fracture of Metals", PP.246~261 Americal Society for Metals (1948)
and
"Studies in Large Plastic Flow and Fracture", Harvard University Press (1964)

2) B.L.Beresuev, L.F.Vereshchogin, Yu.N.Ryabinin and L.D.Livshits
"Some Problems of Large Plastic Deformation of Metals at High Pressures" in Russian, the U.S.S.R. Academy of Sciences (1960)
Translated in English, Pergamon Press (1963)

3) H.L1.D. Pugh, and A.Lt.Low
"The Hydrostatic Extrusion of Difficult Metals", J. Inst. Met. Vol.93 (1964 - 65) PP.201 217

Table 1 Chemical Composition of the Specimens

Carbon Steel

NO.	Standard	Specimen	C	Si	Mn	Cr
1	52100	Bridgman Anvil	1.0	—	—	1.45
2	SUJ-2	Bridgman Anvil	0.95 ~ 1.10	0.15 ~ 0.35	<0.50	1.30 ~ 1.60
3	SK-3	Compression Test Piece	1.00 ~ 1.10	<0.35	<0.50	—

Tungsten Carbide

NO.	Specimen	WC	Co
4	D-Type	97	3
5	B-Type	96.5	3.5
6	T-Type	94	6

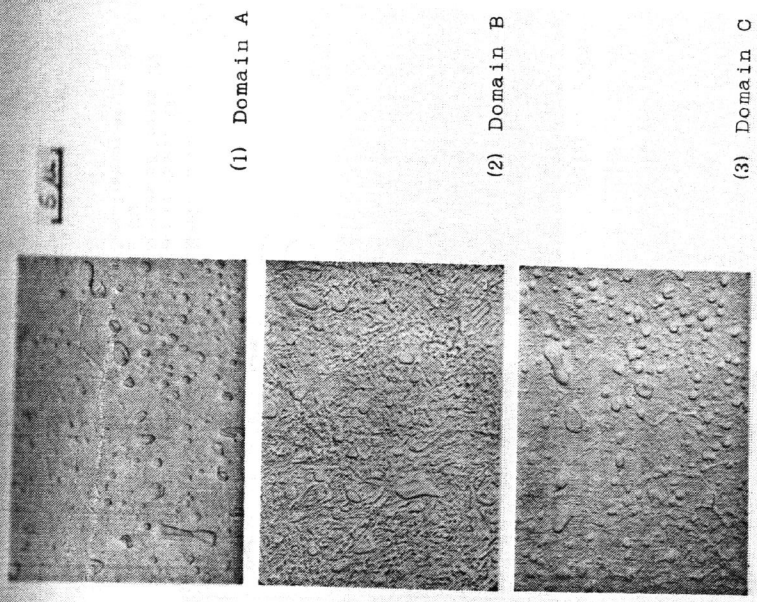

Figure 2 Polished and Etched Surface of the Conical Fragment of 52100 Steel
(1) Domain (A); Nearly Hydrostatically Compressed Region
(2) Domain (B); High Pressure Gradient Region
(3) Domain (C); Nearly Hydrostatic Region but Pressure Lower than Domain (A)

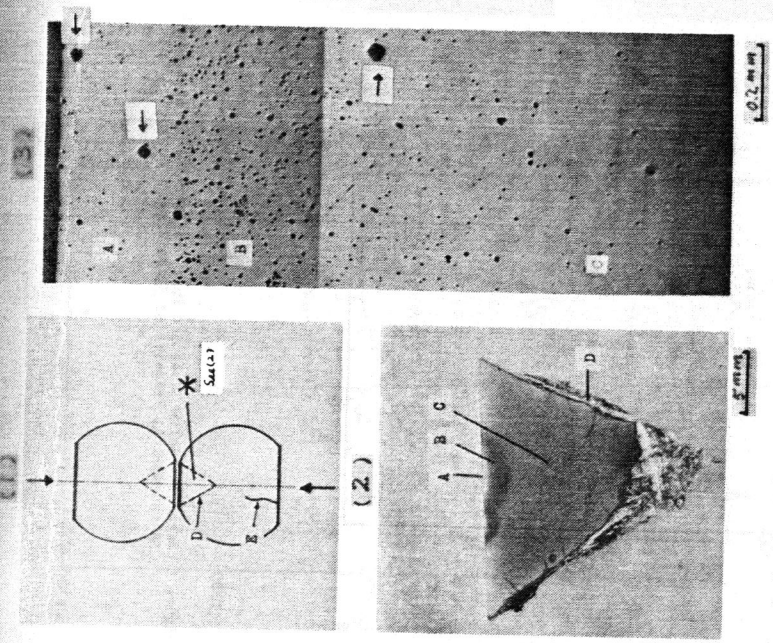

Figure 1 Sectioned Surface of Fragment from Failed 52100 (1% C, 1.45% Cr) Steel under 120 kb
(1) Schematic Figure of Spherical Anvil
(2) Polished and Etched Surface of Fragment Marked with * in (1)
(3) Micrograph of (A), (B) and (C) Domains of the Fragment Arrow marked rectangular pores are indentor marks by the micro-hardness tests.

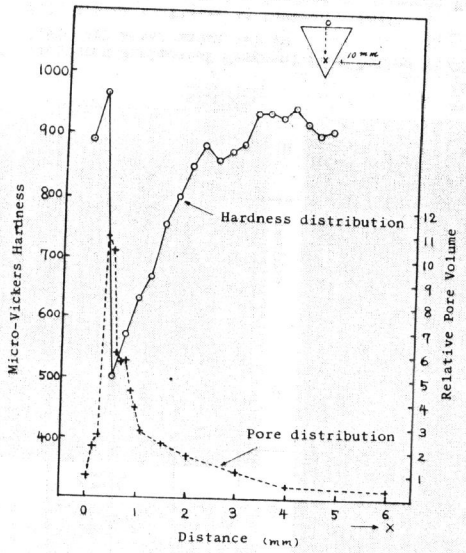

Figure 3 Hardness (Solid Line) and Pore Distribution (Broken Line) in the Conical Fragment of 52100 Steel

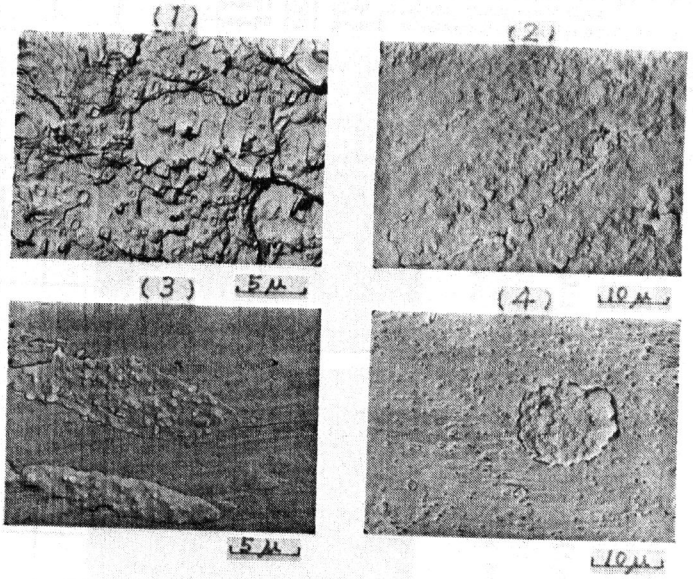

Figure 4 Fractured Surface of 52100 Steel

(1) Brittle-Fractured Surface of Domain (E)
(2) Sheared and Fractured Surface of Domain (D)
(3) Other Portion of Domain (D)
(4) Etched Surface of the Same Portion as in (3)

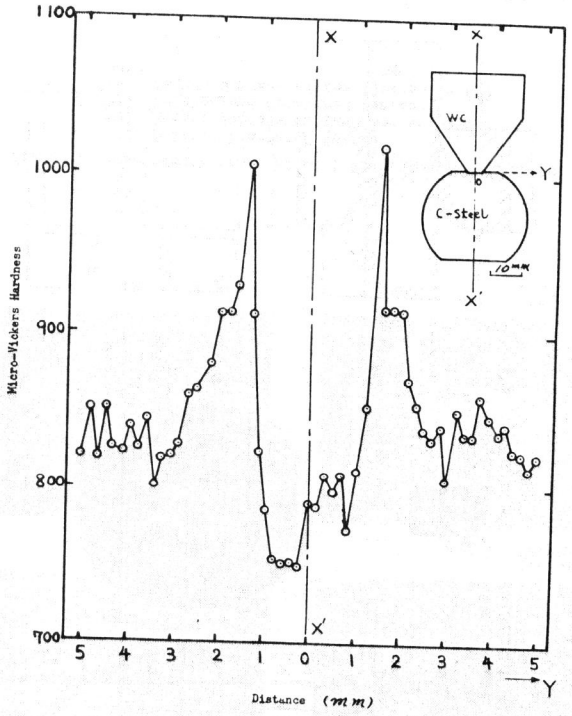

Figure 5 Hardness Distribution in SUJ-2 Steel Spherical Anvil Loaded as the Schematic Figure

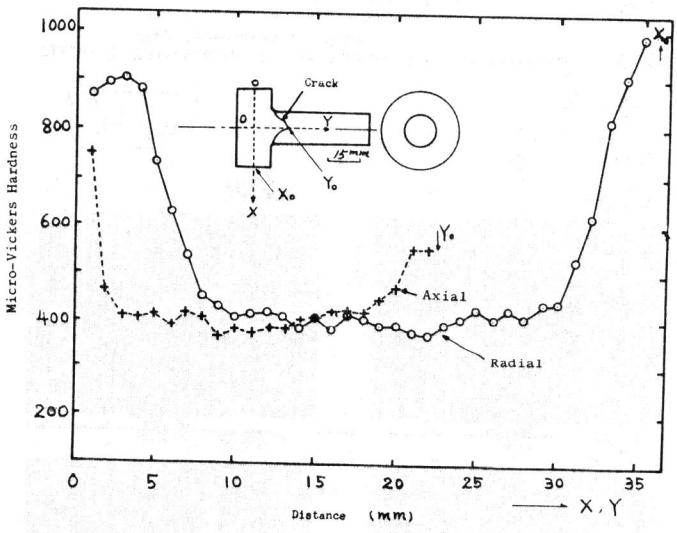

Figure 6 Hardness Distribution in SK-3 Steel Compression Test Piece as Shown in This Figure

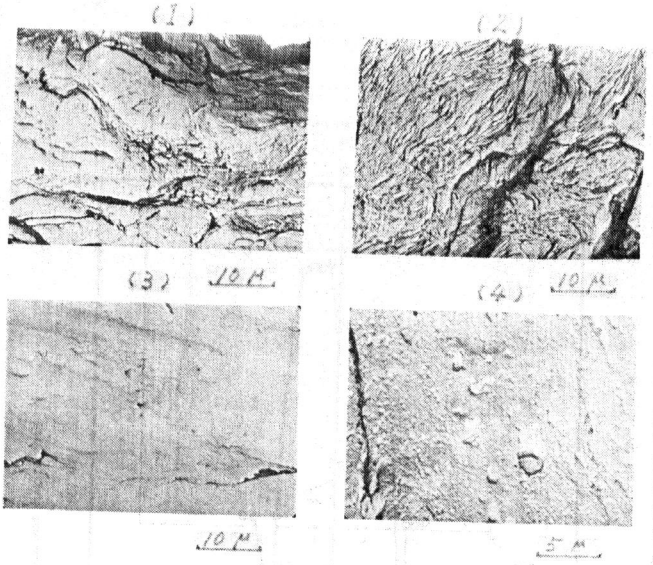

Figure 7 Fractured Surface of SK-3 Steel Compressed to 20 kb
(1) Brittle Fractured Surface
(2) Etched Surface of the Same as in (1)
(3) Sheared and Fractured Surface
(4) Etched Surface of the Same as in (3)

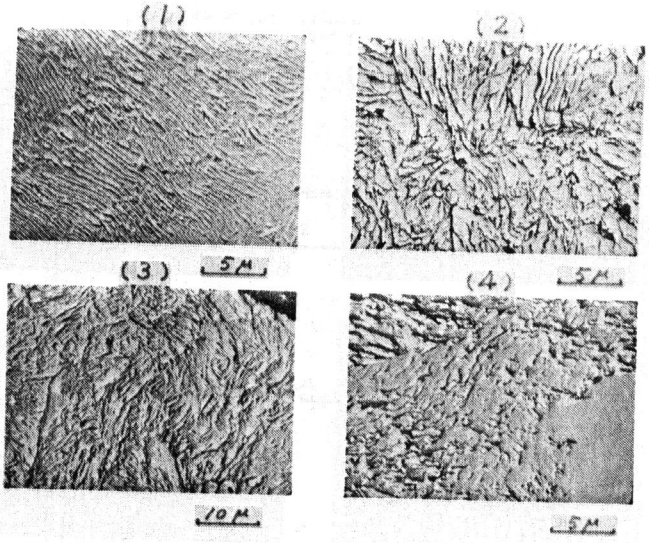

Figure 8 Polished and Etched Surface Near the Fractured Domain of SK-3 Compressed to 20 kb
(1) Compressed but not Flowed
(2),(3) Compressed and Small Flowed
(4) Compresseed and Flowed

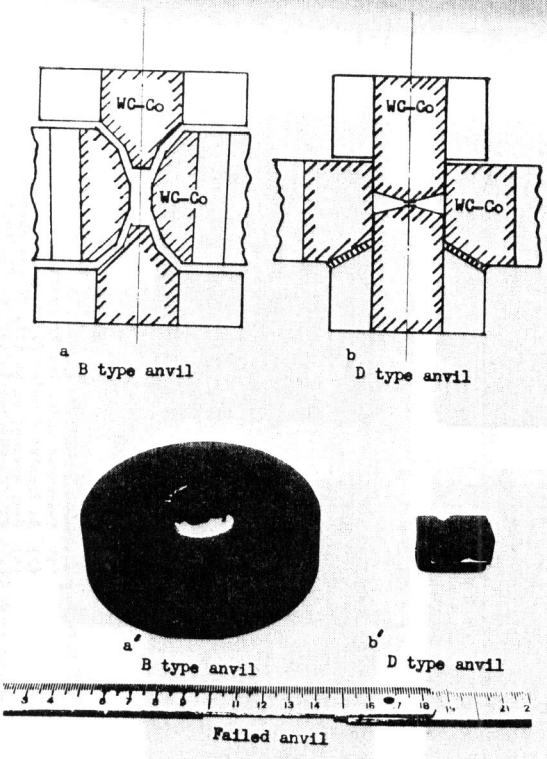

Figure 9 Schematic Figures of Very High Pressure Equipments and Photographs of the Failed Anvils

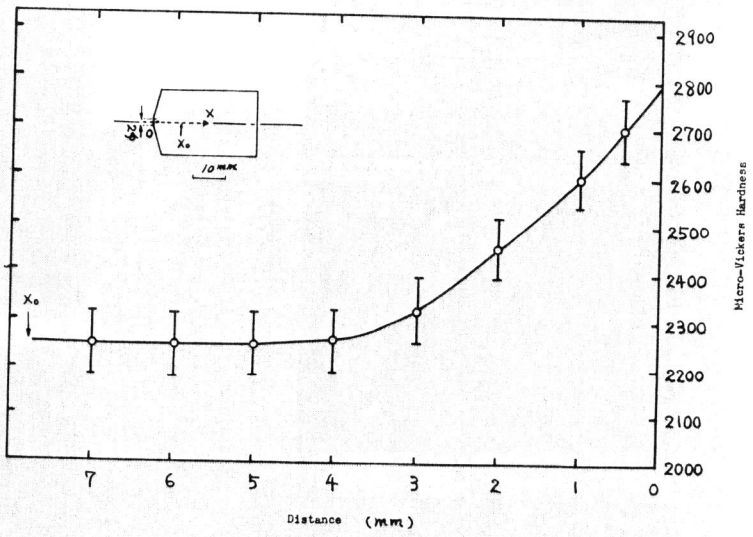

Figure 10 Hardness Distribution in WC-3% Co D-type Anvil Failed at 300 kb as Shown in This Figure

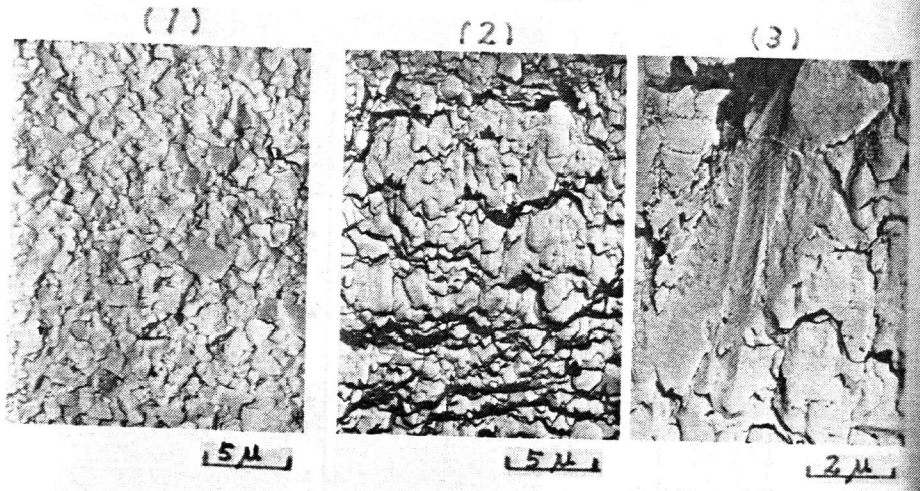

Figure 11 Fractured Surface of WC-3% Co D-type Anvil
(1) Fractured under Low Pressure
(2),(3) Fractured under 300 kb

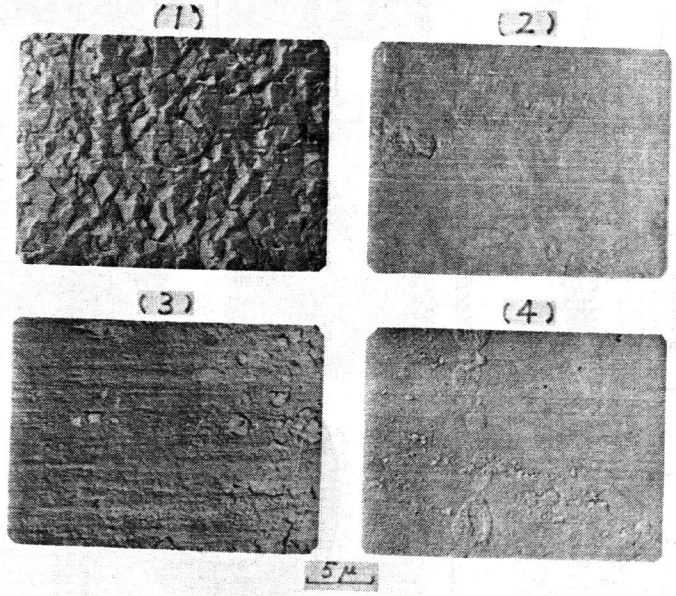

Figure 12 Fractured Surface of WC-3.5% Co B-type Anvil
(1) Fractured under Low Pressure
(2) As Fractured under 70 kb
(3) Same Surface as in (2), WC was Etched
(4) Same Surface as in (2), Co was Etched

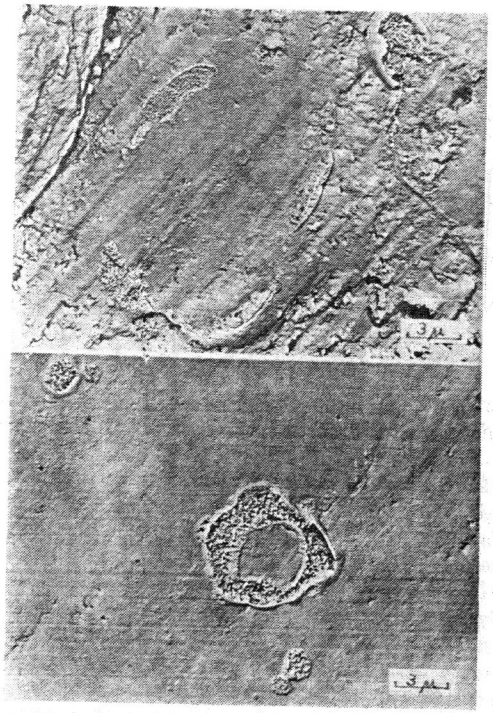

Figure 13 Co-Etched Surface of Failed WC-6% Co T-type Anvil by Shear Force unde 100 kb

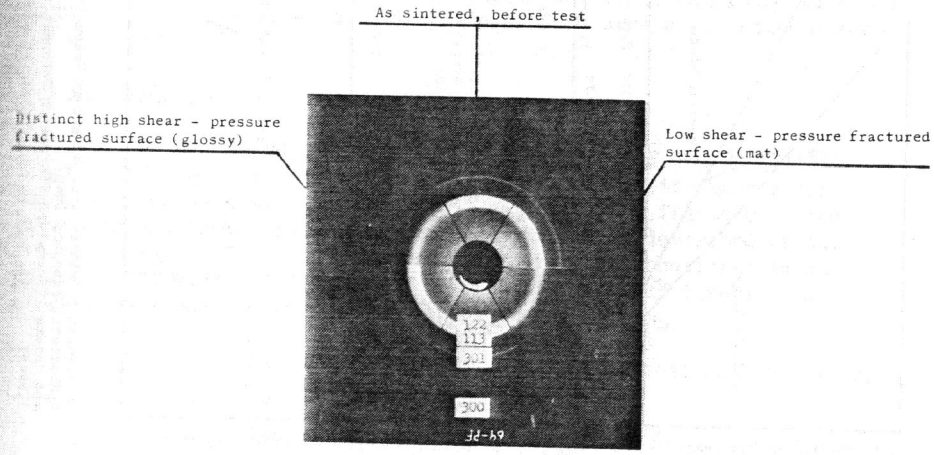

Figure 14 X-Ray Diffraction Pattern of WC-6% Co Sample

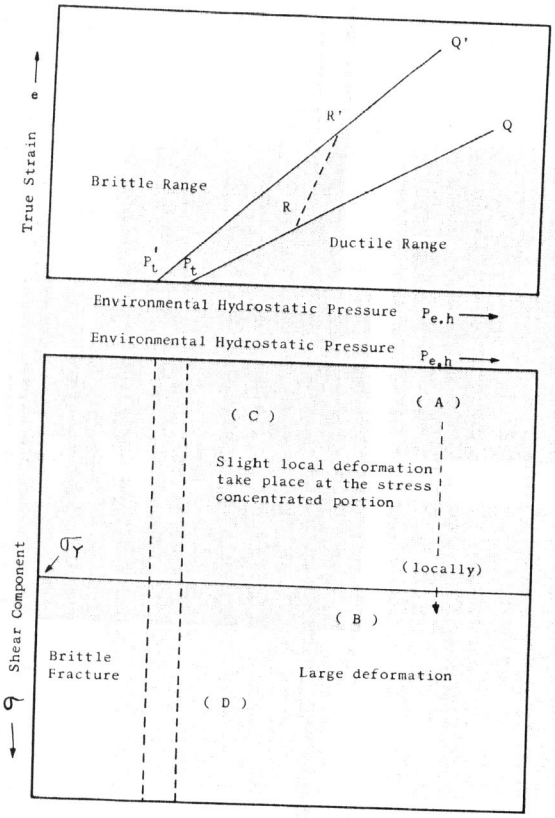

Figure 15 Relationship between True Strain at Fracture and Environmental Hydrostatic Pressure (top) and General Conceptual Diagram of Deformation under Pressure (lower)

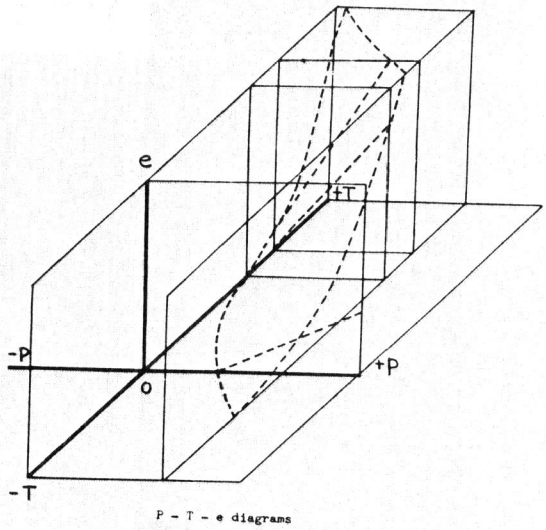

Figure 16 Conceptual Diagram of the Relationships of Pressure (P), Temperature (T) and True Strain at Fracture (e)